J|A|C|S
ARTICLES

Published on Web 03/04/2010

A Guest-Responsive Fluorescent 3D Microporous Metal−Organic Framework Derived from a Long-Lifetime Pyrene Core

Kyriakos C. Stylianou, Romain Heck, Samantha Y. Chong, John Bacsa, James T. A. Jones, Yaroslav Z. Khimyak, Darren Bradshaw,* and Matthew J. Rosseinsky*

Department of Chemistry, University of Liverpool, Liverpool L69 7ZD, U.K.

Received August 2, 2009; E-mail: m.j.rosseinsky@liverpool.ac.uk; deg5y@liverpool.ac.uk

Abstract: The carboxylate ligand 1,3,6,8-tetrakis(*p*-benzoic acid)pyrene (TBAPy)—based on the strongly fluorescent long-lifetime pyrene core—affords a permanently microporous fluorescent metal−organic framework, $[In_2(OH)_2(TBAPy)]\cdot$(guests) (**1**), displaying 54% total accessible volume and excellent thermal stability. Fluorescence studies reveal that both **1** and TBAPy display strong emission bands at 471 and 529 nm, respectively, upon excitation at 390 nm, with framework coordination of the TBAPy ligands significantly increasing the emission lifetime from 0.089 to 0.110 ms. Upon desolvation, the emission band for the framework is shifted to lower energy: however, upon re-exposure to DMF the as-made material is regenerated with reversible fluorescence behavior. Together with the lifetime, the emission intensity is strongly enhanced by spatial separation of the optically active ligand molecules within the MOF structure and is found to be dependent on the amount and chemical nature of the guest species in the pores. The quantum yield of the material is found to be 6.7% and, coupled with the fluorescence lifetime on the millisecond time scale, begins to approach the values observed for Eu(III)-cryptate-derived commercial sensors.

Introduction

Metal−organic frameworks (MOFs) have attracted considerable attention for their large pore volumes accessible through the porous network topologies resulting from the binding of multidentate ligands to metal centers.[1] The ability to chemically modify the ligand either pre- or postsynthesis,[2] combined with the potential for open metal sites,[3] allows the generation of catalytic centers[4] and specific interactions with tailored internal surfaces for applications such as drug delivery[5] and provides exceptional figures of merit for "standard" porous materials applications such as gas storage.[6] The combination of porosity with other properties[7] allows the generation of guest-responsive multifunctional materials from MOFs; however, a combination of significant stable porosity and intense fluorescence in these materials is relatively uncommon. Fluorescent MOFs[8] are of great interest for potential applications as sensors for small molecules,[9] for their use as light-emitting diodes,[10] and in medical diagnostics and cell biology.[11]

MOF fluorescence can be centered on the organic linking group of the framework, particularly if this is highly conjugated, and may be assigned to pure intraligand emission,[12] ligand to metal charge transfer (LMCT),[13] or metal to ligand charge transfer (MLCT).[14] Emission can also be metal-based, usually involving the incorporation of a rare-earth element into the coordination framework,[15] where emission can be enhanced if the organic linker itself functions as an antenna.[16] Guest molecules can also confer fluorescent properties onto MOFs, including through exciplex formation. To date, detailed studies on porous fluorescent MOFs[17] have revealed the influence of

(1) (a) Ferey, G. *Dalton Trans* **2009**, 4400. (b) Kitagawa, S.; Kitaura, R.; Noro, S. *Angew. Chem., Int. Ed.* **2004**, *43*, 2334. (c) Rowsell, J. L. C.; Yaghi, O. M. *Microporous Mesoporous Mater.* **2004**, *73*, 3.

(2) (a) Ingleson, M. J.; Barrio, J. P.; Guilbaud, J. B.; Khimyak, Y. Z.; Rosseinsky, M. J. *Chem. Commun.* **2008**, 2680. (b) Burrows, A. D.; Frost, C. G.; Mahon, M. F.; Richardson, C. *Angew. Chem., Int. Ed.* **2008**, *47*, 8482. (c) Wang, Z. Q.; Tanabe, K. K.; Cohen, S. M. *Inorg. Chem.* **2009**, *48*, 296.

(3) (a) Chen, B. L.; Ockwig, N. W.; Millward, A. R.; Contreras, D. S.; Yaghi, O. M. *Angew. Chem., Int. Ed.* **2005**, *44*, 4745. (b) Choi, E. Y.; Wray, C. A.; Hu, C. H.; Choe, W. *CrystEngComm* **2009**, *11*, 553.

(4) (a) Tanabe, K. K.; Cohen, S. M. *Angew. Chem., Int. Ed.* **2009**, *48*, 7424. (b) Banerjee, M.; Das, S.; Yoon, M.; Choi, H. J.; Hyun, M. H.; Park, S. M.; Seo, G.; Kim, K. *J. Am. Chem. Soc.* **2009**, *131*, 7524.

(5) (a) An, J. Y.; Geib, S. J.; Rosi, N. L. *J. Am. Chem. Soc.* **2009**, *131*, 8376. (b) Horcajada, P.; Serre, C.; Vallet-Regi, M.; Sebban, M.; Taulelle, F.; Ferey, G. *Angew. Chem., Int. Ed.* **2006**, *45*, 5974.

(6) (a) Lin, X.; Telepeni, I.; Blake, A. J.; Dailly, A.; Brown, C. M.; Simmons, J. M.; Zoppi, M.; Walker, G. S.; Thomas, K. M.; Mays, T. J.; Hubberstey, P.; Champness, N. R.; Schroder, M. *J. Am. Chem. Soc.* **2009**, *131*, 2159. (b) Yan, Y.; Lin, X.; Yang, S. H.; Blake, A. J.; Dailly, A.; Champness, N. R.; Hubberstey, P.; Schroder, M. *Chem. Commun.* **2009**, 1025. (c) Ma, S. Q.; Sun, D. F.; Simmons, J. M.; Collier, C. D.; Yuan, D. Q.; Zhou, H. C. *J. Am. Chem. Soc.* **2008**, *130*, 1012. (d) Liu, Y. L.; Eubank, J. F.; Cairns, A. J.; Eckert, J.; Kravtsov, V. C.; Luebke, R.; Eddaoudi, M. *Angew. Chem., Int. Ed.* **2007**, *46*, 3278.

(7) (a) Guo, Z. G.; Cao, R.; Wang, X.; Li, H. F.; Yuan, W. B.; Wang, G. J.; Wu, H. H.; Li, J. *J. Am. Chem. Soc.* **2009**, *131*, 6894. (b) Harbuzaru, B. V.; Corma, A.; Rey, F.; Atienzar, P.; Jorda, J. L.; Garcia, H.; Ananias, D.; Carlos, L. D.; Rocha, J. *Angew. Chem., Int. Ed.* **2008**, *47*, 1080. (c) Vaidhyanathan, R.; Bradshaw, D.; Rebilly, J. N.; Barrio, J. P.; Gould, J. A.; Berry, N. G.; Rosseinsky, M. J. *Angew. Chem., Int. Ed.* **2006**, *45*, 6495.

(8) Allendorf, M. D.; Bauer, C. A.; Bhakta, R. K.; Houk, R. J. T. *Chem. Soc. Rev.* **2009**, *38*, 1330.

the network topology on the fluorescence of conformationally flexible stilbene-based MOFs,[18] whose emission can be irreversibly modified upon guest removal, and shown that guests can control fluorescence wavelengths. More weakly emitting 4,4′,4″-nitrilotris(benzoic acid)-based materials can have their guest-sensitive emissions tuned by the presence or absence of $\pi-\pi$ interactions in desolvated and solvated materials.[19] Such studies now present the opportunity to exploit framework-forming ligands based on cores specifically selected for their desirable optical properties, in particular strong and long-lived emission, that are functionalized to generate large accessible pore volumes. This is an important step in order to design fluorescent materials with the required lifetimes and quantum yields for viable sensing devices.[20]

In this paper we report a new tetracarboxylate ligand, TBAPy, based on the optically active and strongly fluorescent pyrene core as illustrated in Scheme 1, which is functionalized in the 1-, 3-, 6-, and 8-positions with benzoate fragments. (*E*)-Stilbene and pyrene are attractive molecules, due to their use as optical brighteners, dyes, or dye precursors. We have chosen the pyrene core as a linker, as its lifetime and quantum yield (τ = 113 ns,[21] $\phi = 0.65$[22] in EtOH at 293 K) are much higher than those of (*E*)-stilbene (τ = 1.7 ns,[23] $\phi = 0.02$ in acetonitrile[24]), and

Scheme 1. H_4TBAPy Ligand

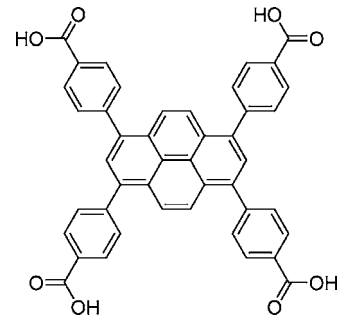

In(III) as the inorganic component to form coordination-based reticular structures with spatially separated pyrene-derived TBAPy fluorophore ligands. Indium has previously been used to prepare topologically diverse MOFs from small carboxylate-based ligands,[25] which have been investigated for hydrogen storage,[6d] ion exchange,[26] and catalysis.[27] It was anticipated that the combination of fluorophore separation in the solid state and the [Kr]4d^{10} configuration of In(III) would limit destructive nonradiative pathways to yield highly emissive permanently porous framework structures.

The reaction of In^{3+} and TBAPy in acidic solution gives a three-dimensional noninterpenetrated porous and strongly fluorescent framework. The specific geometry derived from the ligand and metal ion connectivity affords significant permanent porosity and modulates the ligand−ligand interactions responsible for the optical response. The fluorescent behavior of the framework reversibly responds to the precise nature of the guests (of a range of shapes and sizes permitted by the window and pore sizes) through the position, intensity, and lifetime of the emission. Moreover, the quantum yield and microsecond lifetime of the framework are comparable to those of Eu(III) cryptate based commercial sensors.[28]

Experimental Section

General Information. Reagents and solvents were purchased from Sigma-Aldrich and used as received without further purification. Elemental analyses (C, H, and N) were obtained using a Thermo EA1112 Flash CHNS-O Analyzer. X-ray powder diffraction data were collected in transmission geometry using a STOE Stadi-P diffractometer with Cu Kα radiation at 298 K, except in the case of toluene-loaded **1′**, for which the data were collected at station I11 of the Diamond Synchrotron, U.K., at a wavelength of 0.82633 Å.

Synthesis of 1,3,6,8-Tetrakis(benzoic acid)pyrene (TBAPy) Ligand. Pyrene (5 g, 24 mmol) in 100 mL of nitrobenzene was reacted with excess bromine (5.6 mL, 109 mmol) for 14 h at 120 °C to give 1,3,6,8-tetrabromopyrene. Yield: 98% based on pyrene. The product 1,3,6,8-tetrabromopyrene was judged by solution ^{1}H NMR to be of sufficient purity to be used in the following reaction without further purification.

A mixture of (4-(methoxycarbonyl)phenyl)boronic acid (5 g, 32.9 mmol, 6 equiv), 1,3,6,8-tetrabromopyrene (2.85 g, 5.5 mmol),

(9) (a) Chen, B. L.; Wang, L. B.; Zapata, F.; Qian, G. D.; Lobkovsky, E. B. *J. Am. Chem. Soc.* **2008**, *130*, 6718. (b) Chen, B. L.; Yang, Y.; Zapata, F.; Lin, G. N.; Qian, G. D.; Lobkovsky, E. B. *Adv. Mater.* **2007**, *19*, 1693. (c) Bai, Y.; He, G. J.; Zhao, Y. G.; Duan, C. Y.; Dang, D. B.; Meng, Q. J. *Chem. Commun.* **2006**, 1530. (d) Reineke, T. M.; Eddaoudi, M.; Fehr, M.; Kelley, D.; Yaghi, O. M. *J. Am. Chem. Soc.* **1999**, *121*, 1651.

(10) (a) Stathatos, E.; Panayiotidou, L.; Lianos, P.; Keramidas, A. D. *Thin Solid Films* **2006**, *496*, 489. (b) Kido, J.; Okamoto, Y. *Chem. Rev.* **2002**, *102*, 2357. (c) Wang, J. F.; Wang, R. Y.; Yang, J.; Zheng, Z. P.; Carducci, M. D.; Cayou, T.; Peyghambarian, N.; Jabbour, G. E. *J. Am. Chem. Soc.* **2001**, *123*, 6179.

(11) Altschuh, D.; Oncul, S.; Demchenko, A. P. *J. Mol. Recognit.* **2006**, *19*, 459.

(12) (a) Wang, X. W.; Chen, J. Z.; Liu, J. H. *Cryst. Growth Des.* **2007**, *7*, 1227. (b) Sun, R.; Li, Y. Z.; Bai, J. F.; Pan, Y. *Cryst. Growth Des.* **2007**, *7*, 890.

(13) (a) Zhang, K. L.; Gao, H. Y.; Pan, Z. C.; Liang, W.; Diao, G. W. *Polyhedron* **2007**, *26*, 5177. (b) Song, X. Q.; Liu, W. S.; Dou, W.; Wang, Y. W.; Zheng, M. R.; Zang, Z. P. *Eur. J. Inorg. Chem.* **2008**, 1901.

(14) (a) Frisch, M.; Cahill, C. L. *Dalton Trans.* **2005**, 1518. (b) Gunning, N. S.; Cahill, C. L. *Dalton Trans.* **2005**, 2788.

(15) Huang, Y.; Yan, B.; Shao, M.; Chen, Z. X. *J. Mol. Struct.* **2007**, *871*, 59.

(16) Park, Y. K.; Choi, S. B.; Kim, H.; Kim, K.; Won, B. H.; Choi, K.; Choi, J. S.; Ahn, W. S.; Won, N.; Kim, S.; Jung, D. H.; Choi, S. H.; Kim, G. H.; Cha, S. S.; Jhon, Y. H.; Yang, J. K.; Kim, J. *Angew. Chem., Int. Ed.* **2007**, *46*, 8230.

(17) (a) Xue, M.; Zhu, G. S.; Li, Y. X.; Zhao, X. J.; Jin, Z.; Kang, E.; Qiu, S. L. *Cryst. Growth Des.* **2008**, *8*, 2478. (b) Sun, D. F.; Ke, Y. X.; Collins, D. J.; Lorigan, G. A.; Zhou, H. C. *Inorg. Chem.* **2007**, *46*, 2725. (c) Sun, D. F.; Collins, D. J.; Ke, Y. X.; Zuo, J. L.; Zhou, H. C. *Chem. Eur. J.* **2006**, *12*, 3768.

(18) Bauer, C. A.; Timofeeva, T. V.; Settersten, T. B.; Patterson, B. D.; Liu, V. H.; Simmons, B. A.; Allendorf, M. D. *J. Am. Chem. Soc.* **2007**, *129*, 7136.

(19) Lee, E. Y.; Jang, S. Y.; Suh, M. P. *J. Am. Chem. Soc.* **2005**, *127*, 6374.

(20) (a) Chen, Y. Q.; Bai, H.; Chen, Q.; Li, C.; Shi, G. Q. *Sensors Actuators B-Chem.* **2009**, *138*, 563. (b) Vila-Nova, S. P.; Pereira, G. A. L.; Albuquerque, R. Q.; Mathis, G.; Bazin, H.; Autiero, H.; de Sa, G. F.; Alves, S. *J. Lumin.* **2004**, *109*, 173.

(21) Birks, J. B.; Kazzaz, A. A.; King, T. A. *Proc. R. Soc. London, Ser. A.* **1966**, *291*, 556.

(22) Katoh, R.; Suzuki, K.; Furube, A.; Kotani, M.; Tokumaru, K. *J. Phys. Chem. C* **2009**, *113*, 2961.

(23) Syage, J. A.; Lambert, W. R.; Felker, P. M.; Zewail, A. H.; Hochstrasser, R. M. *Chem. Phys. Lett.* **1982**, *88*, 266.

(24) Mazzucato, U. *Pure Appl. Chem.* **1982**, *54*, 1705.

(25) (a) Volkringer, C.; Loiseau, T.; Ferey, G. *Solid State Sci.* **2009**, *11*, 29. (b) Gao, Q.; Jiang, F. L.; Wu, M. Y.; Huang, Y. G.; Yuan, D. Q.; Wei, W.; Hong, M. C. *CrystEngComm* **2009**, *11*, 918. (c) Huh, S.; Kwon, T. H.; Park, N.; Kim, S. J.; Kim, Y. *Chem. Commun.* **2009**, 4953.

(26) Lin, Z. Z.; Chen, L.; Yue, C. Y.; Yuan, D. Q.; Jiang, F. L.; Hong, M. C. *J. Solid State Chem.* **2006**, *179*, 1154.

(27) Gomez-Lor, B.; Gutierrez-Puebla, E.; Iglesias, M.; Monge, M. A.; Ruiz-Valero, C.; Snejko, N. *Chem. Mater.* **2005**, *17*, 2568.

(28) Bazin, H.; Trinquet, E.; Mathis, G. *Rev. Mol. Biotechnol.* **2002**, *82*, 233.

palladium tetrakis(triphenylphosphine) (0.1 g 0.09 mmol, 1.6 mol %), and potassium carbonate (6 g, 44 mmol, 8 equiv) in dry dioxane (50 mL) was stirred under nitrogen for 72 h at 85 °C. The reaction mixture was poured into a solution of ice containing concentrated hydrochloric acid (3:1). The organic phase was extracted with chloroform, the extract was dried over magnesium sulfate, the solvent volume was reduced under vacuum, and the residue was recrystallized from hot toluene to give an 84% yield of 1,3,6,8-tetrakis(4-(methoxycarbonyl)phenyl)pyrene (3.44 g, 4.6 mmol). Anal. Calcd for $C_{48}H_{34}O_8$: C, 78.04; H, 4.64. Found: C, 77.95; H, 4.81.

A 20 mL portion of concentrated NaOH was added to a suspension of 1 g of 1,3,6,8-tetrakis(4-(methoxycarbonyl)phenyl)pyrene in 100 mL of THF/dioxane/H_2O (ratio 5/2/2) and the mixture was stirred under reflux at 85 °C overnight. The solvent was removed under vacuum, and then H_2O was added to the residue. The mixture (yellow clear solution) was stirred at room temperature for 2 h. The pH value was adjusted to 2 using concentrated HCl. The resulting yellow solid was collected by filtration, washed with water, HCl (1 M), and diethyl ether, and then dried under vacuum. Yield: 0.88 g, 1.29 mmol, 97%. ^{1}H NMR (DMSO-d_6): δ 7.83 (d, J = 8.4 Hz, 8H), 8.06 (s, 2H), 8.14 (d, J = 8.4 Hz, 8H), 8.18 (s, 4H), 13.1 (s, 4H). Anal. Calcd for $C_{44}O_8H_{26}\cdot 1.2H_2O$: C, 75.03; H, 4.06. Found: C, 75.12; H, 4.09.

Synthesis of $In_2(OH)_2(TBAPy)\cdot$(guests) (1). A mixture of $In(NO_3)_3\cdot 9H_2O$ (12 mg 0.03 mmol) and TBAPy (10 mg 0.015 mmol) was dissolved in 4 mL of DMF/dioxane/H_2O (ratio 2/1/1) and 10 μL of concentrated HCl (0.116 mmol) and then sealed in a 12 mL scintilation vial. The vial was heated at 85 °C for 12 h and then cooled to room temperature at a rate of 0.2 °C min^{-1}. The resulting yellow block crystals were isolated in 56% yield (based on In) and washed with DMF in order to remove any recrystallized TBAPy ligand. Anal. Calcd for $In_2C_{44}O_{10}H_{24}\cdot 1.8H_2O\cdot 5.6C_3NOH_7$: C, 52.76; H, 4.86; N, 5.66. Found: C, 52.69; H, 4.93; N, 5.48.

X-ray Crystallography. Single-crystal diffraction data were collected at station 9.8 of the Synchrotron Radiation Source at Daresbury Laboratory, which has a Bruker-Nonius APEXII CCD area detector and D8 diffractometer at an X-ray wavelength of 0.6939 Å. Data were collected at 150 K. The reflection data were integrated using the APEX II software program.[29] The data were corrected for absorption, decay, and other systematic errors using SADABS V2008-1.[30] The structure was solved (by direct methods) and refined using SHELX-97.[31]

Thermogravimetric Analysis (TGA). The experiment was performed under an O_2 atmosphere on a Seiko S-II instrument. A dried crystalline sample was heated at a rate of 5 °C/min up to 650 °C and then cooled to room temperature at a rate of 10 °C/min.

Gas Sorption Measurements. The gas (N_2 and H_2) isotherms of **1** were measured using an Intelligent Gravimetric Analyzer (IGA) from Hiden. The sample was washed with DMF and dried in a desiccator under vacuum overnight. The nitrogen and hydrogen isotherm measurements were performed at 77 K, to a pressure of 1 bar and up to 20 bar, respectively.

Solid-State NMR. All solid-state NMR experiments were conducted at 9.4 T using a Bruker DSX-400 spectrometer operating at 100.61 and 400.13 MHz for ^{13}C and ^{1}H, respectively. All chemical shifts are quoted in ppm from external TMS standard. ^{1}H−^{13}C CP/MAS NMR spectra were acquired at an MAS rate of 10.0 kHz. The ^{1}H $\pi/2$ pulse length was 3.1 μs and a recycle delay of 20 s was used during acquisition. Two-phase pulse modulation (TPPM) decoupling was used during acquisition. ^{1}H−^{13}C variable contact time (VCT) CP/MAS NMR spectra were acquired using contact times in the range of 0.02−12.0 ms. The ^{13}C{^{1}H} MAS NMR spectra were measured at an MAS rate of 10.0 kHz using TPPM decoupling. The ^{13}C $\pi/3$ pulse was 2.6 μs. The spectra were measured using a recycle delay of 30.0 s.

Ultraviolet/Visible Spectroscopy. UV/visible absorbance was collected in the solid state at room temperature on a Perkin-Elmer Lambda 650S UV/vis spectrometer equipped with Labsphere integrating over the spectral range 190−900 nm using $BaSO_4$ reflectance standards. The spectra for **1**, **1′**, and TBAPy were collected by dispersing the same amount of solid in a solid-state holder; the holder for **1′** was filled in the drybox.

Fluorescence Measurements, Quantum Yield, and Lifetime. Fluorescence excitation and emission spectra were collected at room temperature on a Perkin-Elmer LS 55 fluorescence spectrometer. Excitation and emission spectra were collected in the range between 200−600 and 400−700 nm, respectively, with a scan speed of 10 nm/min, and the slits were set at 5.0 (excitation slit) and 6.0 (emission slit). The fluorescence quantum yield for **1** was determined in the solid state according to published procedures.[32] Fluorescence lifetimes were measured using a single flash with a delay of 0.15 ms and gate time of 0.45 ms. Lifetime data were fit using a first-order single expotential with a good quality of fit based on the reduced χ^2 statistics.

Results

Synthesis and Crystal Structure Determination of 1. The reaction of 1,3,6,8-tetrakis(*p*-benzoic acid)pyrene (TBAPy) with $In(NO_3)_3\cdot 9H_2O$ in an acidic DMF/dioxane/H_2O (2/1/1) solvent mixture in a sealed vessel at 85 °C yields pale yellow X-ray-quality single crystals of the fluorescent three-dimensional framework $[In_2(OH)_2(TBAPy)]\cdot$(guests) (**1**). The preparation of **1** is extremely sensitive to synthetic conditions: in order to preclude the formation of an $In(OH)_3$ impurity phase, for example, **1** is prepared for 12 h only. At higher temperatures and longer reaction times, phase-pure samples of **1** are not accessible. The mineralizing agent HCl is required for high yields and crystallinity, and the presence of dioxane aids the solubility of the reactants. While the dioxane does not directly influence the synthesis of **1**, the presence of DMF in the solvent mixture is critical: an exploration of the synthesis of **1** in a range of solvents and solvent mixtures reveals that **1** is only formed in the presence of controlled amounts of DMF, since in pure DMF the TBAPy ligand is recrystallized unreacted.

Framework **1** is based on infinite chains of octahedral $InO_4(OH)_2$ units (Figure 1a), where each In(III) is bound to four TBAPy ligands and two μ_2 trans hydroxide anions (Figure 1b). This is a common coordination motif for M(III) (where M = In, Fe, Cr, Al)[33] with carboxylate ligands and has previously been reported for In frameworks derived from naphthalenetetracarboxylate[34] and 1,2,4,5-benzenetetracarboxylate.[25a] The $InO_4(OH)_2$ chains in **1** are aligned parallel to the crystallographic *b* axis, with the hydroxide and TBAPy carboxylate groups alternating on either side of the chain backbone related by the 2_1 screw axis of the *Cmmm* space group.

The four carboxylate-derived oxygens from the TBAPy ligands form an approximate equatorial square plane around the octahedrally coordinated In (Figure 1b), with a mean $In-O_{carboxylate}$ distance of 2.152(2) Å. The hydroxide bridges

(29) APEX II; Bruker AXS Inc., Madison, WI, 2005.
(30) SADABS Version 2008-2; Bruker AXS Inc., Madison, WI, 2007.
(31) Sheldrick, G. M. SHELX97; University of Göttingen, Göttingen, Germany, 1997.
(32) (a) Wrighton, M. S.; Ginley, D. S.; Morse, D. L. *J. Phys. Chem.* **1974**, *78*, 2229. (b) Ferreira, L. F. V.; Freixo, M. R.; Garcia, A. R.; Wilkinson, F. *J. Chem. Soc., Faraday Trans.* **1992**, *88*, 15.
(33) (a) Loiseau, T.; Mellot-Draznieks, C.; Muguerra, H.; Ferey, G.; Haouas, M.; Taulelle, F. *C. R. Chim.* **2005**, *8*, 765. (b) Serre, C.; Millange, F.; Thouvenot, C.; Nogues, M.; Marsolier, G.; Louer, D.; Ferey, G. *J. Am. Chem. Soc.* **2002**, *124*, 13519.
(34) Volkringer, C.; Loiseau, T.; Guillou, N.; Ferey, G.; Elkaim, E. *Solid State Sci.* **2009**, *11*, 1507.

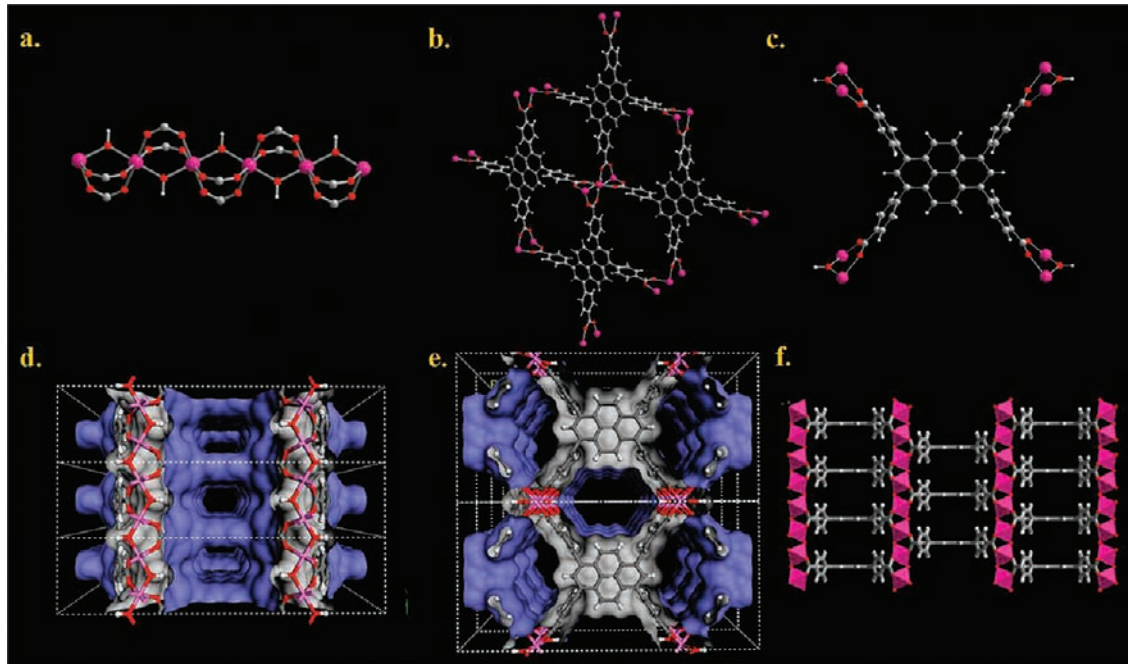

Figure 1. (a) 1D $InO_4(OH)_2$ chains in **1** viewed along the [010] direction. (b) Binding of four different TBAPy ligands to an In(III) center. (c) Coordination mode of the TBAPy ligand in **1**, which binds to eight adjacent indium atoms. (d, e) Connolly surface representations with a probe radius of 1 Å of the 3D noninterpenetrated structure of **1** viewed along the [001] and [010] directions, respectively (gray is outside the surface, and blue is inside the surface). (f) View of the structure of **1** along [001], showing the infinite chains of $InO_4(OH)_2$ units (pink octahedra) connected via the TBAPy ligand (In, pink; C, gray; H, white; O, red).

thus occupy the axial sites, with a slightly shorter mean In−O distance (average 2.056(0) Å) and a bridging In−OH−In angle of 119.90°. The observed In−O distances and the In−OH−In angle are typical for this coordination motif.[25a,33−35]

The $InO_4(OH)_2$ octahedra are corner-shared through the bridging μ_2-OH and are further linked through the TBAPy ligands. The chains are decorated by the TBAPy ligands, which link four of them to form the observed three-dimensional open-framework structure **1** (Figure S1, Supporting Information). Each TBAPy ligand is coordinated to eight adjacent indium atoms (Figure 1c), such that each of the benzoate groups at the 1-, 3-, 6-, and 8-positions of the pyrene core are bound in a bidentate bridging fashion. The benzoate groups themselves are almost orthogonal to the pyrene core with dihedral angles of −104.16 and 74.51°. This perpendicular arrangement of the benzyl substituents arises from the need to prevent steric clashes between the phenyl H atoms in positions 3 or 5 and the pyrene core H atoms in positions 2 and 7, a common arrangement in solid-state structures of 1,3,6,8-tetrabenzyl-substituted pyrenes.[36] The square-grid arrangement of the pyrene cores viewed along [010] arises because each In center binds four TBAPy ligands. The pyrene cores of the TBAPy ligands are eclipsed along [010] and are separated by 7.120(1) Å (Figure 1d), partially enforced by the alternate arrangement of bridging μ_2-OH and ligand carboxylate groups along the length of the $InO_4(OH)_2$ chains.

Framework **1** is a binodal network of stoichiometry $(6\text{-c})_2(8\text{-c})$, since each In(III) is a six-coordinate node (4 × ligands, 2 × μ_2-OH) and each TBAPy is an eight-coordinate node (8 × In) (Figure S2). Topological analysis of **1** using the TOPOS4.0 software package[37] designates this material as a ***sea*** network, using the three-letter notation of O'Keefe.[38] The topology of **1** is comparable with that of other In-based MOFs constructed from tetracarboxylate ligands: e.g., MIL60 and MIL122.[25a,34]

The orientation of the TBAPy ligands around the indium atoms affords an open three-dimensional channel stucture, which can be accessed via all three crystallographic axes. Along [100] access to the porous network is through windows of 5.96 × 2.89 Å (including van der Waals radii). Along [010], however, TBAPy bridging of In centers via the ligand benzoate fragments forms two distinct channels, as shown in Figure 1e, due to the anisotropy of the phenyl substituents on the pyrene unit: the 1−8 separation (5.58 Å) is greater than the 1−3 separation (2.41 Å). The window dimensions for the smaller channel are 4.93 × 9.83 Å and for the larger one are 8.96 × 6.82 Å (see Figure 1e). Along [001] there is only one channel type with window dimensions of 4.84 × 3.72 Å (Figure 1d,f). Despite the large size of the TBAPy ligand, **1** forms a single network that is not interpenetrated, as observed for several MOFs with similarly sized organic linking groups.[39] This is most likely to do with the rigid nature of the pyrene core. The solvent-accessible volume of **1** determined using PLATON is 54%.[40] The large channels in as-made **1** are occupied by crystallographically ill-defined solvent species. Analysis of the residual electron density using the SQUEEZE function within the PLATON suite of

(35) Gandara, F.; Gornez-Lor, B.; Gutierrez-Puebla, E.; Iglesias, M.; Monge, M. A.; Proserpio, D. M.; Snejko, N. *Chem. Mater.* **2008**, *20*, 72.
(36) (a) de Halleux, V.; Calbert, J. P.; Brocorens, P.; Cornil, J.; Declercq, J. P.; Bredas, J. L.; Geerts, Y. *Adv. Funct. Mater.* **2004**, *14*, 649. (b) Zhang, H. J.; Wang, Y.; Shao, K. Z.; Liu, Y. Q.; Chen, S. Y.; Qiu, W. F.; Sun, X. B.; Qi, T.; Ma, Y. Q.; Yu, G.; Su, Z. M.; Zhu, D. B. *Chem. Commun.* **2006**, 755. (c) Bernhardt, S.; Kastler, M.; Enkelmann, V.; Baumgarten, M.; Mullen, K. *Chem. Eur. J.* **2006**, *12*, 6117.
(37) Blatov, V. A.; Shevchenco, A. P.; Russ, V. N. *J. Coord. Chem.* **1995**, *25*, 453. http:/www.topos.ssu.samara.ru.
(38) O'Keeffe, M.; Peskov, M. A.; Ramsden, S. J.; Yaghi, O. M. *Acc. Chem. Res.* **2008**, *41*, 1782.
(39) Kim, J.; Chen, B. L.; Reineke, T. M.; Li, H. L.; Eddaoudi, M.; Moler, D. B.; O'Keeffe, M.; Yaghi, O. M. *J. Am. Chem. Soc.* **2001**, *123*, 8239.
(40) Spek, A. L. *J. Appl. Crystallogr.* **2003**, *36*, 7.

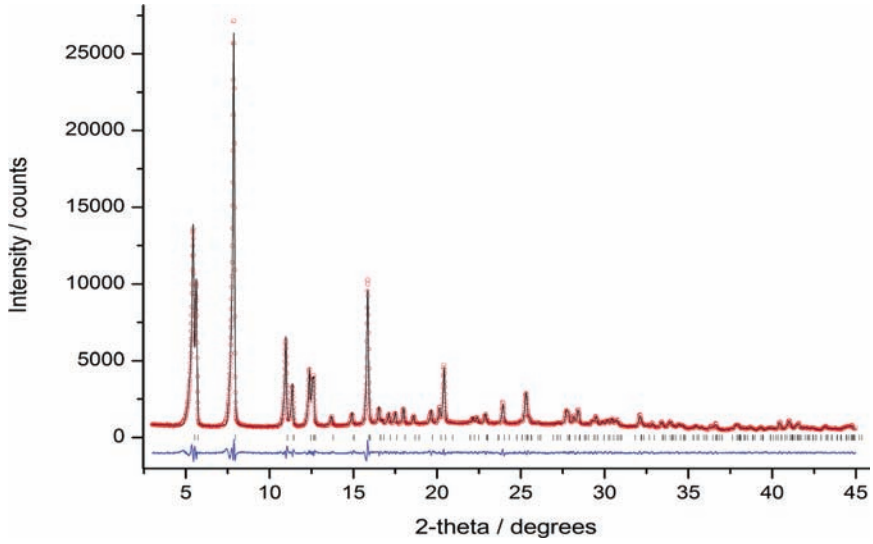

Figure 2. Final observed (circles), calculated (solid line), and difference (below) X-ray powder diffraction profiles for the Le Bail refinement of **1** (R_{wp} = 4.58%, R_P = 3.51%, χ^2 = 1.56; a = 30.8894(9) Å, b = 7.1883(2) Å, c = 15.9833(4) Å, $\alpha = \beta = \gamma = 90°$, *Cmmm*). Reflection positions are marked.

programs[40] indicates the presence of 177.5 electrons per formula unit. This corresponds to three molecules of DMF and four molecules of H_2O (calculated 180 electrons), which is in excellent agreement with the analytical formula and thermogravimetric analysis for bulk phases of **1**.

Bulk Characterization and Thermal Stability of 1. The phase purity and thermal stability of bulk **1** is confirmed from powder X-ray diffraction (PXRD) and thermogravimetric analysis (TGA), respectively. Fitting the PXRD data of **1** according to the Le Bail method yields refined cell parameters a = 30.8894(9) Å, b = 7.1883(2) Å, c = 15.9833(4) Å, and $\alpha = \beta = \gamma = 90°$ with excellent fit indicators (R_{wp} = 4.58%, χ^2 = 1.56) (Figure 2), consistent with those obtained from the single-crystal structure determination (a = 30.748(18) Å, b = 7.120(4) Å, c = 15.932(9) Å at 150 K). **1** is thermally stable to loss of the guest solvent molecules up to 380 °C (Figure S3), yielding the desolvated phase **1′**. Complete desolvation of **1** can also be achieved by outgassing the sample overnight at 150 °C under vacuum using a standard laboratory Schlenk line. While the desolvated material has the same [$In_2(OH)_2$(TBAPy)] framework stoichiometry as **1** (confirmed by elemental analysis; see the Supporting Information), it is clear from PXRD data that there is a structural change and loss of crystallinity upon guest loss. Despite this, the main framework peaks are observed for **1′**, although broadened, with the appearance of additional (broad) peaks at $2\theta \approx 9.2$ and 9.9°. The PXRD profile of **1′** can be indexed with a primitive monoclinic cell (a' = 21.540(2) Å, b' = 31.972(3) Å, c' = 15.626(1) Å, β' = 128.66(1)°, V' = 8403(1) Å^3, *P*2) (Figure S4) related to a monoclinic distortion of the as-made material ($a' \approx 3b$, $b' \approx a$, $c' \approx c$). The desolvated lattice parameters and lowering of symmetry are a clear indication of a loss of structural equivalence on removal of solvent from **1**.

The structural change on going from **1** to **1′** was probed further using solid-state NMR methods, which have previously been shown to be a powerful tool for investigating diamagnetic MOF structures.[19] The $^1H-^{13}C$ CP/MAS NMR spectra and peak assignments of as-made **1** and desolvated **1′** are shown in Figure 3. The spectra of **1** show resonances corresponding to the framework and to encapsulated DMF solvent, all of which display significantly enhanced intensity in the corresponding

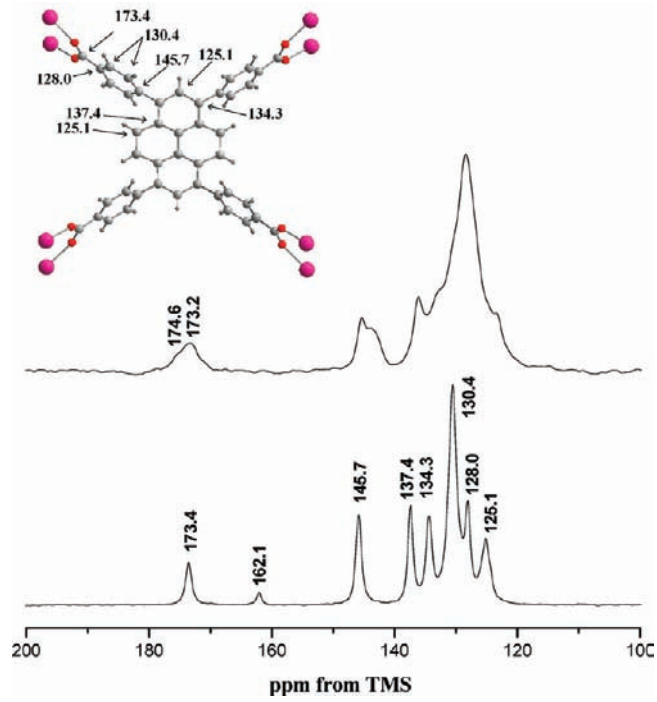

Figure 3. Solid-state CP ^{13}C NMR of **1** (bottom) and **1′** (top) measured at room temperature. The inset shows the assignment of the resonances in **1** to the carbons in the TBAPy ligand. The resonance at 162 ppm in **1** corresponds to the amide carbonyl of DMF, and upon desolvation that resonance is not present. The resulting broadening of the signals upon desolvation is clear.

$^{13}C\{^1H\}$ MAS NMR spectra (Figure S5). The assignment of the framework resonances is entirely consistent with the expected intensities of the lines and $^1H-^{13}C$ CP kinetic experiments (Figure 3). The latter clearly distinguish between H-bearing and quaternary aromatic carbon sites, and the equivalence of the carboxyl groups in **1** is confirmed by the presence of a single resonance at 173.4 ppm.

The complete removal of solvent from **1** is confirmed by the absence of DMF resonances in the spectrum for **1′** and the marked broadening of the signals corresponding to the TBAPy ligand. This can be attributed to rotational rearrangements of

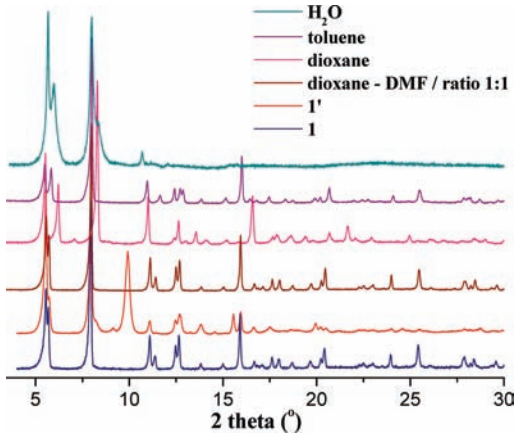

Figure 4. PXRD patterns of the samples produced by loading the fully desolvated sample **1′** with H_2O, toluene, dioxane, and 1/1 DMF/dioxane.

the phenyl rings substituted at the 1-, 3-, 6-, and 8-positions of the pyrene core, leading to dynamic disorder in the structure. Importantly, two nonequivalent sites with approximately equal populations are observable for the carboxylate groups: the chemical shift of the first is identical with that observed in **1**, while the second is shifted downfield to 174.6 ppm. This is indicative of changes in the binding modes of the carboxylate groups upon solvent removal and excludes the possibility of the presence of $-CO_2H$ moieties.[19,41] The resonance at 145.7 ppm, corresponding to the quaternary carbon attached to the pyrene core, also broadens, showing additional features at 144.5 and 143.0 ppm most likely due to the structural nonequivalence of the benzoate groups in desolvated **1′**. This splitting of the carboxylate signal and concomitant broadening of the phenyl ring resonances supports the lowering of symmetry and crystallinity and loss of structural equivalence observed by diffraction methods.

Guest-Dependent Structure of 1. Significantly, the as-made material **1** can be fully recovered after **1′** has been immersed in fresh liquid DMF for 3 h (Figure S6) or mixtures containing DMF (viz. DMF/dioxane 1/1) but is not regenerated on exposure to the other solvents (H_2O, dioxane) that are also used in the synthesis of **1** in their pure forms or small aromatic molecules such as toluene (Figure 4). This reversible structural change on exposure to DMF provides further evidence of its critical role in the formation of open-framework **1**. The other guests do, however, afford materials of different structure and crystallinity. Water has the greatest effect on **1**, and the structure is found to be very sensitive to the number of water molecules present within the porous network (Figure 4). When desolvated **1′** is exposed to the atmosphere, the partially rehydrated phase **1a**, $[In_2(OH)_2(TBAPy)]\cdot 1.6H_2O$, results due to the absorbance of moisture from the laboratory atmosphere. **1a** is found to be slightly less crystalline than **1′**; there are shifts in the peak positions, and some of the lower angle peaks are split with Le Bail profile fitting possible with the cell $a = 15.315(5)$ Å, $b = 16.355(3)$ Å, $c = 15.998(3)$ Å, $\alpha = \beta = \gamma = 90°$, and *Pmmm* (Figure S7). The $^{13}C\{^1H\}$ MAS NMR data (Figure S5) show that **1a** has a level of structural disorder similar to that of **1′**. If, however, **1′** is immersed in water for 30 min, the fully rehydrated material $[In_2(OH)_2(TBAPy)]\cdot 5.9H_2O$ may be prepared with a much higher water loading. The PXRD of fully rehydrated **1** clearly shows a significant loss of crystallinity compared to both **1′** and **1a** (Figure S8), suggesting that increased amounts of water in the porous network lead to significant structural disorder and distortion, with reduction in crystallinity due to the accompanying strain. This reduction in crystallinity suppresses the Bragg diffraction at high angles and frustrates attempts to refine the structure.

Although other guests do not re-form the as-grown structure controlled by DMF, the framework returns to high crystallinity upon addition of nonpolar dioxane or toluene to **1′** (Figure 4), and in both cases the low-angle peak has been split, with the former also exhibiting a broad low-intensity peak at $2\theta \approx 7.1°$. There are also shifts in the positions of the other major Bragg reflections compared to **1**, although the structural changes are less pronounced than those in the case of water discussed above. The PXRD profile of **1′** loaded with dioxane can be indexed with unit cell parameters of $a = 14.332(1)$ Å, $b = 32.398(2)$ Å, $c = 9.446(3)$ Å, $\alpha = 97.30(9)°$, $\beta = 94.75(1)°$, $\gamma = 96.60(7)°$, $V = 4300(5)$ Å^3, and $P\bar{1}$ (Figure S9). The relationship of the cell to as-grown **1**, and the difference from **1′** and **1′**-toluene (see below), shows the range of guest-induced structural change possible.

Elemental analysis of toluene-loaded **1′** indicates that there are 2.1 toluene molecules per $In_2(OH)_2(TBAPy)$ formula unit, consistent with a maximum loading level of 2.7 based on the crystallographically derived pore volume[40] and the liquid density of toluene. Indexing and initial Rietveld refinement required lowering of the crystal symmetry to a related monoclinic cell of similar size to the orthorhombic cell of **1** ($a_m' = 15.6281(7)$ Å, $b_m' = 16.1859(4)$ Å, $c_m' = 14.3261(5)$ Å, $\beta = 76.828(9)°$, $V_m' = 3528.5(1)$ Å^3), using the single-crystal structure of **1** as the starting model. Analysis of the difference Fourier ($F_o - F_c$) map (Figure 5a, inset) shows the location of one toluene molecule with a fractional occupancy of 0.75(3) intercalated between pyrene cores stacked parallel to the $[001]_m$ direction, forming $\pi-\pi$ interactions. Sequential Rietveld refinement of the framework (Figure 5a) and difference Fourier map analysis revealed in total three discrete positions of the toluene guest molecules, accounting for 1.7(1) molecules in the formula unit. Guest molecules occupy both the large and small channels that run parallel to the $[001]_m$ direction with fractional occupancies of 0.40(3) and 0.52(3), respectively (Figure 5b,c)—these molecules are more disordered than those identified in the first Fourier map located between the pyrene cores. In all three cases, the position of the toluene methyl side group is disordered over at least two positions, with strong residual disorder in the case of the 0.52 occupied molecule modeled with an elevated displacement parameter. For the Rietveld refinement, the two para positions with higher density in the Fourier maps were specified and the occupancies split accordingly. The final difference Fourier map indicated no further discrete peaks, indicating that the remaining solvent found analytically is disordered in the channels.

It is clear from the above that the hydrogen-bonding polar guest water has a much greater effect on the structure of **1**, creating more structural disorder relative to the incorporation of nonpolar molecules such as toluene and dioxane into the porous network, though the weaker interactions involving these guests are still able to distort the structure from that adopted in the presence of DMF while reducing the local disorder and resulting strain and loss of crystallinity compared to the water

(41) Chandra, D.; Kasture, M. W.; Bhaumik, A. *Microporous Mesoporous Mater.* **2008**, *116*, 204.

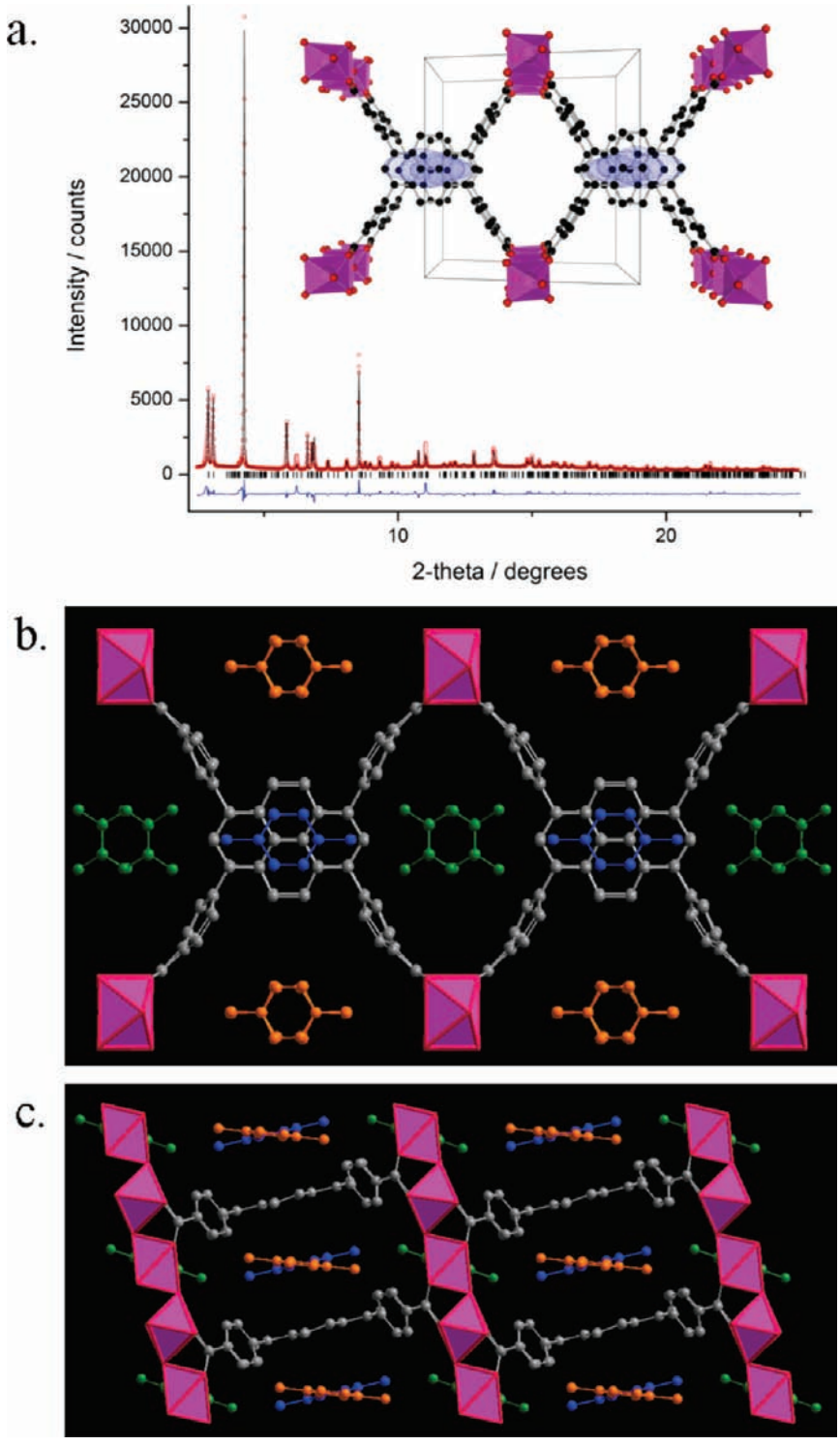

Figure 5. (a) Final observed (circles), calculated (solid red line), and difference (solid blue line) X-ray powder diffraction profiles (298 K) for the Le Bail refinement for the monoclinic sample resulting from toluene loading of **1′** (a_m' = 15.6281(7) Å, b_m' = 16.1859(4) Å, c_m' = 14.3261(5) Å, β = 76.828(9)°, V_m' = 3528.5(1) Å^3, *P*2/*c*, R_{wp} = 8.73%, R_p = 5.41%, χ^2 = 4.36). The inset shows the superposition of observed Fourier-derived scattering density in the first map calculated after refinement of the framework structure of toluene-loaded **1′** viewed along [001], showing the toluene molecules located between the pyrene cores by $\pi-\pi$ interactions. (b) The three refined disordered toluene positions in the structure of toluene-loaded **1′** viewed along [001]. The molecule in blue found in the first Fourier map has a fractional occupancy of 0.75(3), while the less well-localized molecules in the main channels found in subsequent difference Fourier analyses have occupancies of 0.40(3) (green) and 0.52(3) (orange). (c) The three disordered toluene positions viewed along [010].

case. Specific interaction between guest and fluorescent core are revealed by the refined structure of the toluene-loaded material.

Sorption Study. Despite the open framework **1** undergoing a pronounced long-range (XRD) and local (NMR) structural change upon desolvation to **1′**, this material maintains permanent microporosity, as demonstrated by a type I N_2 sorption isotherm (Figure 6). Application of the Brunauer−Emmett−Teller (BET) model in the relative pressure range of p/p^0 0.05−0.30 results in a surface area of 1189(43) m^2/g (Langmuir surface area 1475

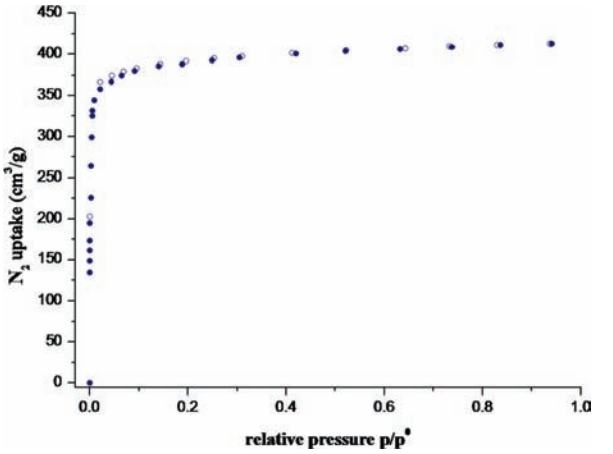

Figure 6. Nitrogen adsorption isotherm of **1′** at 77 K and 1 bar (solid blue circles, adsorption; open blue circles, desorption).

m^2/g). Dubinin−Radushkevich analysis[42] affords a pore volume of 0.639 cm^3/g (Figures S10 and S11), which is slightly larger than that calculated from the single-crystal structure of **1** (0.600 cm^3/g). This difference clearly arises from the observed structural changes between **1** and **1′** and is consistent with the strong guest dependence of the structure discussed above. Gravimetric H_2 sorption data were also recorded (0−20 bar at 77 K, Figure S12) and show that the desolvated framework **1′** reversibly adsorbs 1.16 wt % at 1 bar, increasing to a total uptake of 1.83% at 20 bar.

Optical Properties of 1. UV/vis Spectroscopy. The solid-state UV/vis spectra of **1**, **1′**, and the free TBAPy ligand were recorded under ambient conditions (Figure S13). The TBAPy ligand itself displays strong absorption bands in the UV spectral region from 200 to 500 nm, arising from the $\pi-\pi^*$ transition of the aromatic rings.[43] These bands are not strongly perturbed upon its coordination to In(III); however, a blue shift of 54 nm is observed for the as-made framework **1**. The absorbance of desolvated **1′** shows absorption behavior similar to that of **1**; however, the absorbance maxima are now slightly red-shifted (39 nm) back toward those values observed for the free TBAPy ligand. The clear differences in the absorption spectra between **1** and **1′** must result from the structural changes observed by PXRD and NMR upon desolvation of **1**.

Fluorescence Study. The fluorescence properties of **1**, **1′**, and the TBAPy ligand were also investigated in the solid state at room temperature (Figure 7), and the latter in highly dilute DMF solution (Figure S14). The excitation wavelength of 390 nm was set from the absorption maximum determined from the UV/vis spectral data. A blue shift of 66 nm in the solid-state excitation spectrum was observed (Figure 7) upon coordination of the free TBAPy ligand into the as-made framework **1**, although it is clear that metal binding does not disturb the detailed electronic structure of the UV/vis and excitation spectra, which clearly resemble that of the free TBAPy linker. The free TBAPy ligand fluoresces in the solid state with an emission maximum at 529 nm, whereas TBAPy in DMF solution (8×10^{-9} M) displays a fine structure emission profile that is broader than in the solid state and contains two bands at 386 and 441 nm (Figure S14), blue-shifted relative to the solid-state emission. The fluorescence of as-made **1** displays a strong emission band

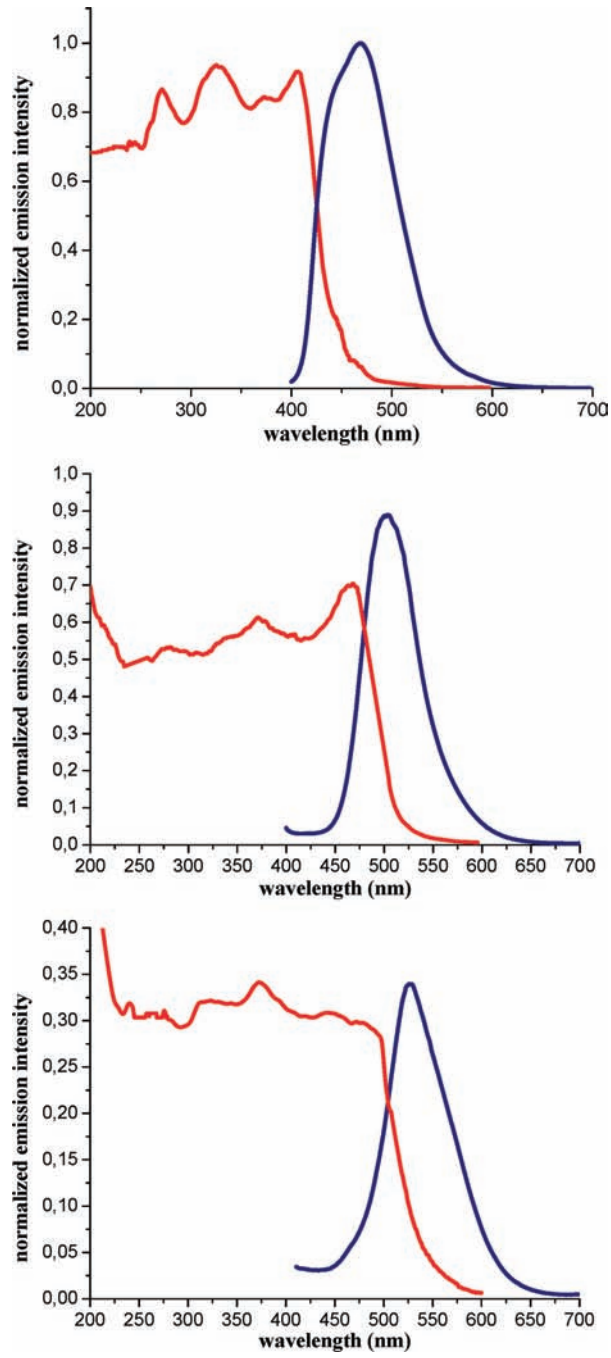

Figure 7. Fluorescence emission (blue) and excitation (red) spectra of **1** (top) and **1′** (middle) and the free TBAPy ligand (bottom) collected in the solid state at room temperature. The emission intensities of **1**, **1′**, and TBAPy are normalized to the maximum emission band of **1**.

at 471 nm with a small shoulder at λ_{max} 445 nm, which is tentatively assigned to a fine-structure emission of the highly diluted free ligand in the framework. Further, the absence of an LMCT band[13b,44] indicates that the observed emission of **1** is generated solely by the ligand.

Upon complete desolvation of **1** to yield **1′**, a 34 nm red shift of λ_{max}, disappearance of the shoulder, and a slight decrease of the emission intensity was observed. Normalization of the solid-

(42) Tovbin, Y. K. *Russ. Chem. Bull.* **1998**, *47*, 637.
(43) Zhou, Y. X.; Shen, X. Q.; Du, C. X.; Wu, B. L.; Zhang, H. Y. *Eur. J. Inorg. Chem.* **2008**, 4280.
(44) (a) Fan, J.; Zhu, H. F.; Okamura, T. A.; Sun, W. Y.; Tang, W. X.; Ueyama, N. *New J. Chem.* **2003**, *27*, 1409. (b) Dai, J. C.; Wu, X. T.; Fu, Z. Y.; Cui, C. P.; Hu, S. M.; Du, W. X.; Wu, L. M.; Zhang, H. H.; Sun, R. O. *Inorg. Chem.* **2002**, *41*, 1391.

state emission spectra to the maximum emission intensity observed for **1** indicates that the emission of **1′** is decreased by 10% but both framework structures display higher emission intensity than the free TBAPy ligand. The fluorescence lifetime of **1** was determined to be $\tau = 0.1100 \pm 0.0027$ ms (Figure S15 and Table 1), significantly longer than those reported for other fluorescent MOFs which are often on the nanosecond time scale.[18,45] It is noteworthy that the lifetime of **1** is also longer than that observed for the solid-state emission of the uncoordinated TBAPy ligand, whereas the lifetime of **1′** is slightly shorter than that of TBAPy. This indicates that the fluorescence lifetime is enhanced in the as-made framework but that a slight change in structure upon desolvation returns this to the level observed for the free ligand, even though the emission intensity of **1′** remains 2.5× higher.

Quantum yield, Φ_f, is a measure of the emission efficiency of a fluorochrome and is defined as the number of photons emitted divided by the number of photons absorbed. The quantum yield (Figure S16) of **1** is 6.7% and is smaller than that reported for some MOFs; for example, the quantum yields reported for 2-D square grid structures based on Zn(II) and norfloxacin are >20%, although their fluorescent lifetimes remain very short at 10^{-9} s.[45] In the present case, however, the coupling of the modest quantum yield with a microsecond fluorescence lifetime is comparable with a number of Eu(III) cryptates,[46] some of which have been labeled with biomarkers and found utility as commercial sensors for the detection of biological analytes through homogeneous time-resolved fluorescence (HTRF) or time-resolved amplified cryptate emission (TRACE).[28]

Guest-Dependent Fluorescence of 1. It is known that some fluorescent MOF materials exhibiting linker-centered emission are sensitive to the presence or absence of guest solvent molecules[18,47] and their exact chemical nature.[19] In order to investigate the role of DMF in the formation of **1** and the time course evolution of the structural regeneration (**1′** to **1** in the presence of DMF), the desolvated framework **1′** was exposed to anhydrous DMF solvent over a range of different times and emission spectra of the DMF solvates recorded. A blue shift of 19 nm is observed with respect to the emission band of **1′**, for a sample exposed to DMF for 5 min only. After 3 h, however, the position of λ_{max} (474 nm) returns to the wavelength recorded for as-made **1**, clearly indicating the reversible access of DMF molecules in the cavity to regenerate the emission profile of **1** within this time (Figure 8). Further, a weak shoulder at 426 nm appeared for the 5 min exposed sample and became more intense after 3 h, consistent with the ligand fine-structure emission observed in as-made **1**. The lifetime of the DMF-loaded samples follows the same trend as the emission intensity (Table 1), increasing from 0.0890 ± 0.0023 ms in the case of the desolvated material, **1′**, to 0.1100 ± 0.0027 ms for the 3 h DMF exposed material.

We have further examined the sensitivity of the emission response of **1** to the other solvents employed in the synthesis (viz. dioxane and H_2O) and also to the presence of an aromatic guest molecule (toluene) (Figure 9 and Table 1). After activation, desolvated **1′** was immersed in the liquid solvents for 30 min prior to measurement (experimental details are given in the Supporting Information). Exposure of **1′** to H_2O induces the largest shift of λ_{max} (520 nm) relative to as-made **1**, which is comparable to that observed for the free TBAPy ligand. Further, there is a quenching of the emission intensity to $I = 0.72$ compared to the maximum emission of **1**. The fluorescence lifetime of this material, at 0.054 ms, is approximately 50% of that observed for as-made **1**. The shift in the position of the emission band and the reduction of emission intensity and lifetime are dependent on the amount of water present in the framework, since the partially hydrated material (**1a**) has a λ_{max} and lifetime similar to those of desolvated **1′**, whereas the emission intensity is only 50% of that observed for the fully desolvated material and 63% of that for the hydrated phase (Table 1). Clearly the fluorescence response of the framework is sensitive not only to water but also to the number of guest water molecules present within the porous network and, thus, the changes in both structure and structural order noted above. At low loadings of water (1.6 per FU) longer lifetimes are recorded but emission intensity is reduced, whereas at higher loadings (5.9 per FU) the intensity is almost restored to that observed for **1′** but the lifetime is much reduced. This is related to the differences observed in structure between the partially and fully (re)hydrated samples of **1′**.

Immersion of **1′** in anhydrous dioxane results in a smaller shift in λ_{max}, to 502 nm, but induces a significant quenching of the emission intensity ($I = 0.36$), comparable to that of free TBAPy (Table 1). The fluorescence lifetime of **1′** reloaded with dioxane is 0.064 ms, much lower than that determined for **1′** (0.081 ms) or the free TBAPy ligand (0.089 ms) but higher than that recorded for rehydrated **1′** (0.0540 ms). It is clear that both H_2O and dioxane have a dramatically different effect on the emission of **1** when compared to each other or anhydrous DMF under the same conditions: exposing **1′** to DMF for 30 min shifts λ_{max} by 6 nm only, and the emission intensity is almost equal to that of as-made **1**, the spectrum being further character-

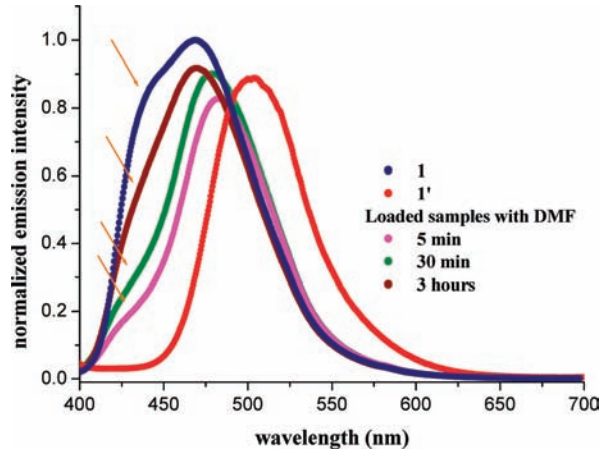

Figure 8. Effect of DMF molecules on the fluorescence characteristics of **1** (**1** dark blue, **1′** red, exposure of **1′** to DMF for 5 min pink, for 30 min green, and for 3 h brown). The emission profiles of the samples loaded with DMF are blue-shifted with enhanced emission intensity compared to **1′**. The λ_{max} value of **1′** exposed to DMF for 3 h is the same as that of **1**. The orange arrows show the appearance of the shoulder for the DMF-loaded sample after 5 min exposure, which becomes more intense after 3 h. For ease of comparison, the emission intensity is normalized to the maximum intensity observed for the as-made material, **1**.

(45) Chen, Z. F.; Xiong, R. G.; Zhang, J.; Chen, X. T.; Xue, Z. L.; You, X. Z. *Inorg. Chem.* **2001**, *40*, 4075.
(46) (a) Bazzicalupi, C.; Bencini, A.; Berni, E.; Bianchi, A.; Giorgi, C.; Fusi, V.; Valtancoli, B.; Lodeiro, C.; Roque, A.; Pina, F. *Inorg. Chem.* **2001**, *40*, 6172. (b) Chen, Q. Y.; Feng, C. J.; Luo, Q. H.; Duan, C. Y.; Yu, X. S.; Liu, D. J. *Eur. J. Inorg. Chem.* **2001**, 1063. (c) Sabbatini, N.; Guardigli, M. *Coord. Chem. Rev.* **1993**, *123*, 210.
(47) Huang, Y. Q.; Ding, B.; Song, H. B.; Zhao, B.; Ren, P.; Cheng, P.; Wang, H. G.; Liao, D. Z.; Yan, S. P. *Chem. Commun.* **2006**, 4906.

Table 1. Fluorescence Characteristics of $[In_2(OH)_2(TBAPy)]\cdot(guests)$[a]

material and treatment	refined guest composition from analytical data	emission band (nm)	lifetime (ms)	emission intensity	quantum yield (%)
TBAPy		529	0.0890 ± 0.0023	0.34	
1	5.6DMF, 1.8H_2O	445 sh, 471	0.1100 ± 0.0027	1.00	6.7
1′		505	0.0810 ± 0.0012	0.88	
1a	1.6H_2O	501	0.0810 ± 0.0019	0.42	
1′ for 5 min in DMF	4.2DMF	426 sh, 486		0.82	
1′ for 30 min in DMF	4.6DMF	428, 480	0.0990 ± 0.0033	0.89	
1′ for 3 h in DMF	4.9DMF	431 sh, 474	0.1100 ± 0.0015	0.92	
loaded **1′** in toluene	2.1(toluene)	486	0.0670 ± 0.0028	0.71	
loaded **1′** in dioxane	2.9(dioxane)	502	0.0640 ± 0.0016	0.36	
loaded **1′** in DMF/ dioxane	3.5DMF, 0.6(dioxane)	446 sh, 485	0.0980 ± 0.0012	0.89	
loaded **1′** in H_2O	5.9H_2O	520	0.0540 ± 0.0021	0.72	

[a] sh = shoulder band.

ized by a shoulder at 428 nm (Figure 8). It is notable that this shoulder, assigned to ligand fine-structure emission, is not present when **1′** is exposed to either H_2O or dioxane. As dioxane appears to have a large effect on both the lifetime and the emission intensity compared to DMF, we also investigated the immersion of **1′** in a dioxane/DMF 1/1 solvent mixture. We reasoned that in the presence of controlled amounts of DMF—as in the synthesis of **1**—the effects on the fluorescence properties would be less pronounced than for dioxane alone. Indeed, after immersion of **1′** in the 1/1 DMF/dioxane mixture for 30 min, the emission profile more closely resembles that observed for the sample reloaded with only DMF (for 30 min), indicating that its influence on the structure and hence fluorescent characteristics of framework **1** is more far-reaching than that of any other of the solvents investigated.

An aromatic solvent molecule was also loaded into **1′**, to see if the emission response was affected by species that have the potential to interact directly with the highly aromatic TBAPy component of the framework through $\pi-\pi$ interactions. Exposure of **1′** to toluene caused a blue shift in λ_{max} of 19 nm (relative to **1′**) and a quenching of the emission intensity by 30% of that recorded for **1** (Figure 9 and Table 1). The emission band is blue-shifted compared to the desolvated material and is no broader than in the presence of other solvents; therefore, it is unclear whether this is attributable to exciplex emission[48] in the present case: this cannot be completely ruled out, however, due to the demonstrable interactions between toluene and the pyrene cores of TBAPy determined from toluene-loaded **1′** (Figure 5). Concomitant with the shift of λ_{max} is a reduction in the fluorescence lifetime from 0.1100 ms in **1** to 0.0670 ms, a value comparable to reloading **1′** with dioxane (see Table 1). Although the lifetimes for the dioxane- and toluene-loaded samples are similar, the shift of the emission band and the reduction in intensity are much less for toluene than for dioxane. This most likely indicates that these guests interact with the framework in different ways depending on their exact chemical nature—since they are of similar polarity as reflected in their dielectric constants of 2.21 and 2.38, respectively, for dioxane and toluene—and induce a similar structural change in **1**.

The toluene-loaded **1′** sample can be reactivated at 100 °C for 18 h under vacuum in a Schlenk tube and re-exposed to liquid DMF for a further 12 h. The resulting PXRD (Figure S19) confirms that the slight shift of the Bragg peaks and the splitting of the low-angle peak observed in the toluene-loaded material are absent and that phase-pure **1** was recovered, as further evidenced by the maximum emission band of 470 nm, equal to λ_{max} for **1** (Figure S20).

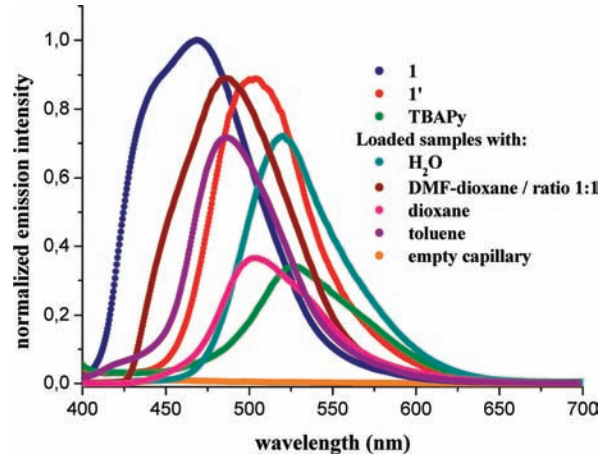

Figure 9. Guest-dependent fluorescence emission spectra of **1** (dark blue), **1′** (red), and TBAPy (green) and samples of **1′** loaded with DMF/dioxane (brown), dioxane (pink), toluene (purple), and H_2O (sky blue). The shoulder noted in Figure 8 in the presence of DMF molecules does not occur for the dioxane-, toluene-, and H_2O-loaded samples. For ease of comparison, the emission intensity is normalized to the maximum intensity observed for the as-made material, **1**. The emission spectrum of an empty capillary collected under the same parameters as the loaded samples is shown in yellow.

Discussion

The thermally stable open-framework structure **1** is composed of highly conjugated pyrene-derived TBAPy fluorophore ligands linked into a three-dimensional network by chains of corner-sharing $InO_4(OH)_2$ octahedra. While the pyrene cores of the TBAPy organic linking groups are relatively rigid, the benzoate groups substituted at the 1-, 3-, 6-, and 8-positions have a degree of rotational freedom, allowing the structure of **1** to respond to small guest molecules. The structural arrangement of the TBAPy ligands in **1** electronically isolates the optically active pyrene cores while simultaneously exposing them to the large solvent-accessible extra-framework volume (Figure 1e): coupled with the ability of the open framework to respond to changes in the composition and nature of the solvent molecules within its pore stucture, this has significant implications for the fluorescence properties of this material.

The as-made framework **1** does not display any metal−ligand or ligand−metal charge transfer (MLCT and LMCT, respectively) bands in its fluorescence emission spectra, consistent with the fluorescent response of the framework being determined only

(48) (a) Wagner, B. D.; McManus, G. J.; Moulton, B.; Zaworotko, M. J. *Chem. Commun.* **2002**, 2176. (b) McManus, G. J.; Perry, J. J.; Perry, M.; Wagner, B. D.; Zaworotko, M. J. *J. Am. Chem. Soc.* **2007**, *129*, 9094.

by the TBAPy ligands, such that the emission is linker-centered.[15] This is evidenced by the similarity of the UV−vis and excitation spectra of **1** with those of the free TBAPy linker; although the excitation spectrum is blue-shifted by 66 nm compared to the ligand, this is expected due to the increased separation of the fluorophores in the coordination framework resulting in a decrease of the $\pi-\pi^*$ energy gap. A similar trend is observed in cubic MOFs with linker-centered emission, where organic linkers of increasing conjugation display the greatest blue shift of the emission band.[18] It is the high degree of conjugation in the pyrene core of the TBAPy ligands and position of the energy levels in In(III)[49] that ensures the fluorescence of **1** is centered on the ligand; if less-conjugated chromophores are employed, the charge transfer to the metal is significantly more efficient and LMCT bands could be observed.[13b,44] The ligand-centered emission of **1** is consistent with fluorescent In(III) MOFs containing 2,2′-bipyridyl ligands[50] and octahedral dipyrrinato complexes of group 13 metal ions.[49]

Electronic interactions between polyaromatic molecules in the solid state are known to strongly control their optical properties through $\pi-\pi$ interactions,[51] which can lead to quenching of the emission intensity.[52] The intensity of the lowest energy (0−0) emission peak of solid-state TBAPy at 529 nm, however, can be enhanced by a factor of 3 upon coordination in as-made framework **1**. This is indicative of a significantly decreased interaction between the pyrene cores and results from their 7.12 Å spatial separation within the three-dimensional open framework structure, a distance that precludes the specific $\pi-\pi$ interactions that can lead to emission quenching. This effect can also be achieved by decreasing the interchromophore coupling by highly diluting a solution of the optically active centers, and indeed a 10^{-9} M DMF solution of TBAPy displays fine structure in its emission profile and is blue-shifted compared to its solid-state emission.

As demonstrated, the complete desolvation of **1** to **1′** induces a 34 nm red shift of the emission band and modest quenching of the fluorescence. This is consistent with increased interactions between the optically active TBAPy linkers and must be attributable to the structural rearrangements of **1** upon desolvation, as observed by PXRD and NMR spectroscopic studies. This has previously been observed in $Zn_4O(NTB)_2\cdot 3DEF\cdot EtOH$ (where NTB = 4,4′,4″-nitrolotris(benzoate))[19]and $Zn_4O(SDC)_3$ (where SDC = 4,4′-stilbenedicarboxylate),[18] where interactions between two interpenetrated nets are enhanced upon guest solvent removal, such that desolvation allows the linkers to rotate or change conformation to increase their proximity, causing a concomitant increase in $\pi-\pi$ interactions red-shifting the fluorescence emission maxima. Although **1** is not an interpenetrated structure, it does exhibit significantly less long-range order on desolvation (to **1′**) due to a loss of structural equivalence, particularly of the benzoate groups substituted in the 1-, 3-, 6-, and 8-positions of the pyrene core. It is unlikely that the planar pyrene cores, rigidly held in place by the chains of corner-shared $InO_4(OH)_2$ octahedra, will be able to approach sufficiently closely to interact with one another without an enormous structural rearrangement. While the refined cell parameters of desolvated **1′** do indicate structural change and a reduction in symmetry, such a significant rearrangement clearly does not occur. We therefore attribute the observed red shift and 10% decrease in intensity and lifetime to rotations of the benzoate groups as seen in the $^{13}C\{^1H\}$ MAS NMR data, which have the potential to increase the degree of conjugation, thus red-shifting the emission.[45] Such enhancement of conjugation would be consistent with the loss of interactions with guests as a factor determining the conformation of the TBAPy ligand.

The emission band of **1** is clearly sensitive to structural changes induced by rotations of the TBAPy benzoate donor groups, but it is also influenced by the presence and chemical nature of guest solvent molecules within the pores (Figure 9). This is common for MOFs with linker-centered emission, where a solvatochromic effect in the fluorescence emission spectra dependent on the polarity of the included solvent molecules can occur.[19] The size of the shift is dependent on the chemical nature of the guest and how this interacts with the organic linking group of the framework, which may lead to emission quenching.[9c] The emission response of the desolvated material **1′** to each of the solvents employed in the synthesis of the framework was examined, as was an aromatic guest molecule (toluene) that could potentially interact directly with the linker through $\pi-\pi$ interactions. Most notably, the presence of DMF in the pores of desolvated **1′** causes the structure of as-made **1** to be regenerated, indicating that the structural change and fluorescence characteristics are fully reversible, a desirable property for the formation of sensors. The increase in lifetime of **1′**, the enhancement of the intensity of the fluorescence signal, and the appearance of fine-structure emission upon exposure to DMF are due to the nature of the three-dimensional structure of **1** and its specific interactions with the polar DMF guest molecules.

In contrast with the reversible changes in structure and fluorescence behavior between **1** and **1′** upon exposure of the desolvated material to DMF, the other guest molecules examined (water, dioxane, and toluene) do not regenerate the structure nor reproduce the fluorescence characteristics of as-made **1**. Undoubtedly, the exact response is related to the complex interplay between the chemical nature of the solvent (e.g., polarity, aromaticity) and the extent to which this can change the structure of **1**. Polar guest molecules, for example, have the greatest influence on the structure of framework **1** in comparison to nonpolar guests, as demonstrated by the loss of long-range order on exposure of **1′** to water.

With respect to the emission characteristics of **1′** exposed to solvent molecules for 30 min, it appears that polar guests have the greatest effect on the fluorescence lifetime with an accessible range of $\Delta_{lifetime} = 0.045$ ms, in comparison with $\Delta_{lifetime} = 0.003$ ms for nonpolar guests. Conversely, the nonpolar guests exert the greatest influence on the emission intensity with $\Delta_{intensity} = 0.33$, wheras polar guests have $\Delta_{intensity} = 0.18$. The lifetime therefore appears more sensitive to changes in structure upon adsorption of polar molecules, whereas the intensity is more sensitive to specific interactions with nonpolar guests. The latter is evidenced by our ability to locate specific guests in the toluene-loaded structure of **1′** that clearly sit between the highly conjugated pyrene cores of the framework. The exception to this is the partially hydrated sample **1a**, where low levels of water do not change the lifetime significantly but severely reduce the intensity. This may be related to specific water-binding sites in close proximity to the framework structure of **1**, which are occupied at low loadings of the guest. The differences in the position of the emission maxima are attributed to a solvochro-

(49) Thoi, V. S.; Stork, J. R.; Magde, D.; Cohen, S. M. *Inorg. Chem.* **2006**, *45*, 10688.
(50) Tian, Z. F.; Song, T. Y.; Fan, Y.; Shi, S. H.; Wang, L. *Inorg. Chim. Acta* **2007**, *360*, 3424.
(51) Cornil, J.; Beljonne, D.; Calbert, J. P.; Bredas, J. L. *Adv. Mater.* **2001**, *13*, 1053.
(52) Cornil, J.; dos Santos, D. A.; Crispin, X.; Silbey, R.; Bredas, J. L. *J. Am. Chem. Soc.* **1998**, *120*, 1289.

matic effect, but these do not correlate particularly with solvent polarity, as previously observed by Bauer et al.[18]

The presence of DMF in the pores of **1** produces a highly ordered and well-defined structure in which TBAPy ligands are spatially isolated from one another such that the interaction between them is comparable to those in highly dilute solutions. Reproduction of the shoulder attributed to fine-structure emission of the TBAPy ligand in as-made **1** only occurs with DMF, which has the smallest effect on the structure despite its polarity. In addition to a specific role for DMF in the synthesis of **1**, this suggests that the ligands are at their most dilute in the framework when DMF is present. This arrangement is disturbed due to structural changes or specific interactions with the pyrene core upon adsorption of other guests; therefore, the fine-structure emission band is not observed. The reversibility of the optical behavior upon loading of DMF following desolvation to form **1′**, loading, and then unloading of the toluene confirms the reversible access of DMF in the pores and its essential role in the formation of the original lifetime and minimization of self-quenching.

Conclusion

The judicious combination of a highly fluorescent pyrene-derived ligand with a d^{10} metal ion that is known to form networks sustained by inorganic clusters and chains[6d,25a] yields a highly emissive, permanently porous three-dimensional framework, **1**, that displays good quantum yield and a millisecond fluorescent lifetime. In the present case, the combination of linker-based fluorescence with large robust pores and a BET surface area >1000 m^2/g in a single framework—desirable properties previously restricted to fluorescent MOFs based on lanthanoid emission[16,53]—allows the emission wavelength, lifetime, and intensity of **1** to be tuned for a wide variety of guest species and loadings: the resulting changes in lifetime and fluorescence intensity are consistent with, respectively, the influence of the guest on the structure and the chemical nature of the guest itself.

Polar aprotic DMF produces a high degree of structural order and separates the linkers to minimize self-quenching phenomena, resulting in a fine-structure emission profile. Removal of this guest disorders and alters the conformation of the benzoate groups—consistent with NMR data and the observed red-shifting of the emission—increasing structural disorder. Although loss of DMF clearly reduces crystallinity and local order, the porosity apparent from the structure of as-grown **1** is completely retained (judged by the sorption-derived pore volume) in desolvated **1′**. The hydrogen-bonding capabilities of the polar water guest confer qualitatively distinct characteristics from DMF to strongly distort the structure, possibly due to interaction with the carboxylate groups, which become inequivalent when the DMF (around which the structure forms) is removed. The structural distortions induced by the interaction with polar guests strongly affect the lifetime of the emission.

Nonpolar dioxane and toluene guests both produce less distortion of the framework structure than water, but the specific π-stacking revealed by diffraction allows toluene to strongly interact with the fluorescent pyrene core, reducing the emission intensity. The sensitivity of the fluorescence to the aliphatic dioxane is surprising but reflects the role of multiple weak interactions in controlling MOF structures where there are no dominant bonds.

The ligand design, with a long lifetime fluorescent core in guest-controllable interactions with its surrounding benzoate groups, combines guest sensitivity due to direct interactions with the ligand itself and via guest-induced framework distortions with the capability of accessing large-pore structures such as those in the MIL and IRMOF families. The potential chemical tunability of linker-based fluorescence would allow for considerable enhancement of the guest sensitivity observed here.

Acknowledgment. We thank the EPSRC for funding under EPSRC/C511794 and the support of the European Union under the 6th Framework Program; keyword SURMOF. We gratefully acknowledge Dr. A. M. Fogg, Dr. J. Rabone, and Mr. J. A. Gould for assistance with the Connolly surface plots and topological analysis, respectively.

Supporting Information Available: Text, figures, and tables giving TGA, PXRD, and solid-state ^{13}C NMR data, emission spectra, quantum yields, and lifetime plots, and a CIF file giving crystallographic data for **1**. This material is available free of charge via the Internet at http://pubs.acs.org. CCDC 740938 also contains supplementary crystallographic data for this paper. These data can be obtained free of charge from The Cambridge Crystallographic Data Centre (CCDC) via www.ccdc.cam.ac.uk/data_request/cif.

JA906041F

(53) Devic, T.; Serre, C.; Audebrand, N.; Marrot, J.; Ferey, G. *J. Am. Chem. Soc.* **2005**, *127*, 12788.